Journal of Magnetic Resonance 202 (2010) 57–63

Contents lists available at ScienceDirect

Journal of Magnetic Resonance

journal homepage: www.elsevier.com/locate/jmr

Line-narrowing in proton-detected nitrogen-14 NMR

Simone Cavadini [a], Veronika Vitzthum [a], Simone Ulzega [a,*], Anuji Abraham [a,1], Geoffrey Bodenhausen [a,b]

[a] Institut des Sciences et Ingénierie Chimiques, Ecole Polytechnique Fédérale de Lausanne, Batochime 1530, CH-1015 Lausanne, Switzerland
[b] Département de Chimie, associé au CNRS, Ecole Normale Supérieure, 24 rue Lhomond 75231, Paris Cedex 05, France

ARTICLE INFO

Article history:
Received 14 August 2009
Revised 28 September 2009
Available online 30 September 2009

Keywords:
Solid-state NMR
Magic angle spinning (MAS)
^{14}N
HMQC
HSQC
Homonuclear dipolar decoupling
Symmetry-based pulse sequence

ABSTRACT

In solids spinning at the magic angle, the indirect detection of single-quantum (SQ) and double-quantum (DQ) ^{14}N spectra ($I = 1$) via spy nuclei $S = 1/2$ such as protons can be achieved in the manner of heteronuclear single- or multiple-quantum correlation (HSQC or HMQC) spectroscopy. The HMQC method relies on the excitation of two-spin coherences of the type $T^I_{11}T^S_{11}$ and $T^I_{21}T^S_{11}$ at the beginning of the evolution interval t_1. The spectra obtained by Fourier transformation from t_1 to ω_1 may be broadened by the homogenous decay of the transverse terms of the spy nuclei S. This broadening is mostly due to homonuclear dipolar S–S' interactions between the proton spy nuclei. In this work we have investigated the possibility of inserting rotor-synchronized symmetry-based C or R sequences and decoupling schemes such as Phase-Modulated Lee–Goldburg (PMLG) sequences in the evolution period. These schemes reduce the homonuclear proton–proton interactions and lead to an enhancement of the resolution of both SQ and DQ proton-detected ^{14}N HMQC spectra. In addition, we have investigated the combination of HSQC with symmetry-based sequences and PMLG and shown that the highest resolution in the ^{14}N dimension is achieved by using HSQC in combination with symmetry-based sequences of the R-type. We show improvements in resolution in samples of L-alanine and the tripeptide ala-ala-gly (AAG). In particular, for L-alanine the width of the ^{14}N SQ peak is reduced from 2 to 1.2 kHz, in agreement with simulations. We report accurate measurements of quadrupolar coupling constants and asymmetry parameters for amide ^{14}N in AAG peptide bonds.

© 2009 Elsevier Inc. All rights reserved.

1. Introduction

Because of the ubiquity of nitrogen in a wide range of materials, and because of its structural and functional role in many proteins and nucleic acids, it would be attractive to obtain spectroscopic signatures of ^{14}N in a straightforward manner. In contrast to popular nuclei with $S = 1/2$ such as ^{13}C and ^{15}N, ^{14}N has a spin quantum number $I = 1$ and a challenging quadrupole coupling constant on the order of a few MHz [1–4]. In spite of these adverse conditions, ^{14}N spectroscopy appears to be on the verge of becoming a routine technique, thanks to indirect detection via neighboring spy nuclei with $S = 1/2$ such as ^{13}C or ^{1}H combined with magic angle spinning (MAS). In heteronuclear multiple-quantum correlation (HMQC) [5–14], it is possible to transfer coherence from S to I nuclei via second-order quadrupole–dipole cross-terms [15,16], also known as residual dipolar splittings (RDS) [9,11], via scalar couplings [10,14], or via recoupled heteronuclear dipolar interactions by using rotary resonance [14,17–20]. Recoupling can be achieved by applying a continuous radiofrequency (*rf*) field to the spy nucleus $S = 1/2$ with an *rf* amplitude that is a multiple of the rotor spinning frequency, i.e., $\omega^S_1 = n\omega_{rot}$ with $n = 1$ or 2. Alternatively, symmetry-based RN sequences of the $R20_5^9$ type [21,22] can recouple the heteronuclear dipolar I–S (^{14}N–^{1}H) interactions while simultaneously decoupling the homonuclear S–S' interactions [23]. It was found by van Beek et al. [24] that the $R18_2^5$ method was also efficient to recouple heteronuclear dipolar ^{17}O–^{1}H interactions, and Brinkmann et al. [25,26] showed that it is possible to obtain accurate measurements of ^{17}O–^{1}H distances by supercycling the shorter $R4_1^2$ sequence. Proton-detected HMQC experiments suffer from line-broadening due to homonuclear dipolar S–S' (^{1}H–^{1}H) interactions in both ω_1 and ω_2 dimensions. The quest for high-resolution proton spectra in solid-state NMR has lead to the development of sophisticated methods for decoupling homonuclear dipolar ^{1}H–^{1}H interactions. Recent progress in the design of MAS probes for very fast spinning, currently up to about 70 kHz, makes it possible to attenuate these homonuclear interactions significantly [27]. The combination of fast MAS with multiple pulse sequences, known as "combined rotation and multiple pulse spectroscopy" (CRAMPS) [28], requires synchronization with the rotor period $\tau_{rot} = 1/\nu_{rot}$, as in modified WHH4 sequences [29] or symmetry-based $R18_2^9$ sequences [30,31]. Synchronization is not a particular problem in the present context, since the t_1

* Corresponding author. Fax: +41 21 6939435.
E-mail address: simone.ulzega@epfl.ch (S. Ulzega).
[1] Present address: Department of Chemistry, Durham University, Durham, UK.

1090-7807/$ - see front matter © 2009 Elsevier Inc. All rights reserved.
doi:10.1016/j.jmr.2009.09.018

increments have to be rotor-synchronized anyway to eliminate the large first-order ^{14}N quadrupolar broadening. On the other hand, one can chose methods that do not require any synchronization, such as Lee–Goldburg (LG) experiments [32] from which frequency-switched LG (FSLG) [33,34] and Phase-Modulated Lee–Goldburg (PMLG) [35–39] techniques have been derived. An alternative to these methods is offered by the DUMBO decoupling scheme [40], which leads to efficient decoupling over a wide range of spinning speeds [41,42]. Recently, Amoureux et al. have shown that efficient homonuclear dipolar proton decoupling can be achieved at high spinning speeds by applying smooth amplitude modulated (SAM) pulse sequences [43,44].

In this work, we used rotor-synchronized symmetry-based sequences [21,22] and PMLG schemes [35–39] during the evolution interval t_1 of HMQC and HSQC pulse sequences to reduce the ^{1}H–^{1}H dipolar interactions, and consequently obtain line-narrowing in the indirect ω_1 dimension of SQ and DQ ^{14}N spectra. We show that a substantially improved resolution can be achieved by merging HSQC methods with symmetry-based sequences of the *R*-type.

2. Experimental

Samples of L-alanine ($^{14}NH_3^+C^\alpha H^\alpha C^\beta H^\beta{}_3COO^-$) and the tripeptide alanine–alanine–glycine (AAG, $NH_3^+C^\alpha HCH_3CONHC^\alpha HCH_3CONHC^\alpha H_2COO^-$, ^{13}C labeled in all three C^α positions) were purchased from Cambridge Isotope Laboratories. These samples were packed in a 2.5 mm outer diameter ZrO_2 rotor with a sample volume of ca. 11 μl. The spectra were obtained at 9.4 and 18.8 T, where the ^{1}H (^{14}N) Larmor frequency appears at 400 (28.9) and 800 (57.8) MHz, respectively. The rotors were spun at 30.03 or 31.25 kHz, either in a wide-bore Bruker triple resonance CP-MAS probe at 9.4 T (400 MHz for ^{1}H) or in a narrow-bore Bruker triple resonance CP-MAS probe at 18.8 T (800 MHz). In the former case, the magic angle was adjusted within 0.01° using deuterated α-oxalic[D_6] acid [45]; in the latter we used KBr to adjust the angle. The *rf* amplitude of the ^{14}N pulses was calibrated by direct detection of $^{14}NH_4NO_3$, which has a very small quadrupole splitting. Using a 1 kW amplifier, the ^{14}N pulses had an amplitude of ν_r^N = 57 kHz. The details of the *C*, *R* and PMLG sequences are given below.

3. Applications

In L-alanine the ^{14}N nucleus in the rapidly rotating ammonium group only has a modest quadrupolar constant, which we have estimated [9] to be C_Q = 1.13 MHz with η_Q = 0.28. In the $^{14}NH_3^+$ group, the heteronuclear dipolar coupling between the three ammonium protons (which act together as spy nuclei) and the ^{14}N nucleus, when 'recoupled' by the $R20_5{}^9$ sequence [46,47], is expected to be on the order of 1–2 kHz. This interaction is partly overshadowed by the homonuclear *S*–*S*′ dipolar couplings between the ammonium $^{14}NH_3^+$ protons, the nearby H^α, the more remote H^β protons and other protons belonging to neighboring molecules in the crystal lattice [27]. In the excitation and reconversion intervals, these interactions can be attenuated by appropriate *R*-type symmetry-based sequences, which simultaneously decouple the homonuclear *S*–*S*′ dipolar couplings while recoupling the heteronuclear *S*–*I* interactions. Homonuclear *S*–*S*′ couplings that act during t_1 can be suppressed by *C*-, *R*-type symmetry-based sequences or other homonuclear dipolar decoupling methods such as PMLG, DUMBO and SAM. In particular, PMLG and DUMBO perform best when the decoupling cycle time τ_c is *not* a multiple of the rotor period [41,42]. Here we have investigated the performance of a non-synchronized PMLG scheme. SAM is expected to be less efficient at high MAS frequencies [48].

4. Recoupling heteronuclear interactions

In all HMQC and HSQC experiments with L-alanine, we applied the $R12_3{}^5R12_3{}^{-5}$ rotor-synchronized pulse sequence [21,22] to protons *S* in the excitation and reconversion intervals τ_{exc} and τ_{rec} in order to recouple the heteronuclear dipolar *S*–*I* interaction. We shall refer to R-HMQC and R-HSQC in these cases, where *R* indicates that we use symmetry-based sequences of the *R*-type to recouple heteronuclear dipolar interactions. This is shown in Fig. 1a and b. This windowless sequence consists of a sixfold repetition in 3 rotor periods of the pulse pair $\{180_{75}\ 180_{285}\}_6$, i.e., 12 pairs of π pulses with phases ϕ = 75° and 285°. To ensure that the sequence is less sensitive to *rf* phase shift errors, phase-inverted supercycles [22,49] were used. Therefore the $R12_3{}^5$ element is followed by a $R12_3{}^{-5}$ element where the signs of all phases are reversed. This supercycle reduces the number of second-order terms in the average Hamiltonian [46,49]. To further improve the performance of the recoupling of the heteronuclear dipolar *S*–*I* interactions, nested supercycles may be implemented as shown by Brinkmann et al. for ^{17}O–^{1}H pairs [25,26]. In experiments with AAG, the highest coherence transfer efficiency was obtained using the shorter $R12_3{}^5$ pulse sequence.

5. Decoupling homonuclear *S*–*S*′ interactions in the indirect dimension

We have applied $R6_1{}^3$ and $C6_2{}^3$ pulse sequences to protons *S* in the evolution interval t_1 to decouple the homonuclear dipolar *S*–*S*′ interactions. If we opt for the R-HMQC scheme in combination

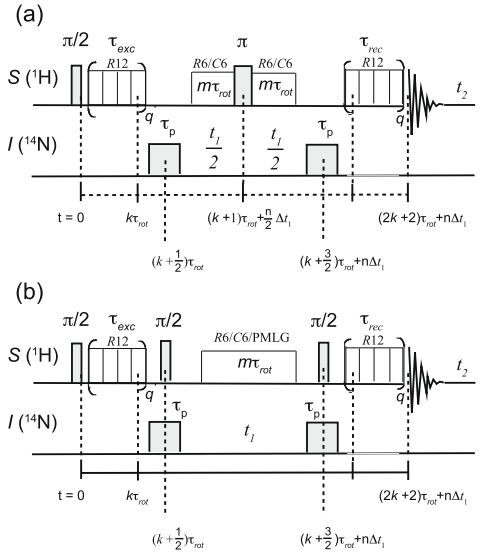

Fig. 1. (a) R-HMQC pulse sequence combined with homonuclear proton decoupling schemes for the indirect observation of ^{14}N SQ or DQ spectra. The rotor-synchronized *R*12 recoupling pulse scheme starts after a delay $1/(8\tau_{rot})$ after the initial $\pi/2$ pulse. A repeating block with four π pulses as represented in (a) requires $q = k = 3, 6, 12, \ldots$. The dashed lines show the synchronization. For both the $C6_2{}^3$ and the $R6_1{}^3$ sequences, the first point of the 2D spectrum (i.e., $n = 0$) is obtained with $t_1 = \tau_{rot} = 1/\nu_{rot}$, whereas the following points are obtained by incrementing $t_1 = n\Delta t_1$ (with $n = 1, 2, \ldots$) in steps $\Delta t_1 = 2/\nu_{rot}$ for $R6_1{}^3$ and $\Delta t_1 = 4/\nu_{rot}$ for $C6_2{}^3$. When $C6_2{}^3$ is used, *m* takes values $2(n-1)$, whereas for $R6_1{}^3$ *m* takes values $(n-1)$, with $n = 1, 2, \ldots$. (b) R-HSQC pulse sequence combined with homonuclear proton decoupling schemes for the indirect observation of ^{14}N SQ or DQ spectra. The excitation and reconversion conditions are similar to (a). During t_1, for both the $C6_2{}^3$ and the $R6_1{}^3$ sequences, the first point of the 2D spectrum (i.e., $n = 0$) is obtained with $t_1 = \tau_{rot} = 1/\nu_{rot}$, whereas the other points are obtained by incrementing $t_1 = n\Delta t_1$ (with $n = 1, 2, \ldots$) in steps $\Delta t_1 = 1/\nu_{rot}$ for $R6_1{}^3$ or $\Delta t_1 = 2/\nu_{rot}$ for $C6_2{}^3$. When $C6_2{}^3$ is used, *m* takes values $2(n-1)$, whereas for $R6_1{}^3$, *m* takes values $(n-1)$, with $n = 1, 2, \ldots$. The phase cycles are available from the authors upon request.

with the $R6_1^3$ sequences, the latter must be inserted before and after the refocusing π pulse applied in the middle of the t_1 evolution period (Fig. 1a). Each $R6_1^3$ sequence consists of 3 pairs of π pulses with phases $\phi = 90°$ and 270°, i.e., six π pulses in one rotor period. On the other hand, the $C6_2^3$ windowless sequence consists of 3 pairs of 2π pulses per rotor period with phases $\phi = 0°$ and 180°. Each $C6_2^3$ sequence needs two full rotor periods to be completed. In R-HMQC experiments the advantage of $R6_1^3$ is thus that the smallest time increment required is $\Delta t_1 = 2\tau_{rot}$, i.e., half of what is needed for $C6_2^3$, which requires $\Delta t_1 = 4\tau_{rot}$. Consequently, the spectral width in the ω_1 dimension can be twice as large for $R6_1^3$ as for $C6_2^3$.

If we opt for the R-HSQC scheme in combination with homonuclear decoupling schemes, the latter must be inserted between the two $\pi/2$ pulses applied to protons (Fig. 1b). In R-HSQC experiments the smallest time increment is given by the number of rotational periods, e.g., $\Delta t_1 = \tau_{rot}$ for $R6_1^3$ and $\Delta t_1 = 2\tau_{rot}$ for $C6_2^3$.

6. Results and discussion

Fig. 2 shows the ^{14}N SQ (top) and DQ (bottom) 2D R-HMQC spectra of L-alanine ($^{14}NH_3^+CHCH_3COO^-$) obtained at 9.4 T. In addition to the strongest signal due to the ammonium protons of the NH_3^+ group, it is possible to observe weaker signals of other protons. The latter are weak compared to the ammonium protons because of the low efficiency of coherence transfer from remote ^{1}H to ^{14}N and back.

Long-range correlations may in principle be observed by increasing the excitation and reconversion intervals. The three ammonium protons, which rotate rapidly about the N–C^α axis, act together as three spy nuclei with $S = 1/2$ each, with a group spin $S = 3/2$. The efficiency of coherence transfer of the R-HMQC and R-HSQC methods can be estimated from the ratio

$$r = S_{SQ/DQ}/S_{spin\text{-}echo}. \quad (1)$$

This ratio compares the signal amplitude $S_{SQ/DQ}$ of the first row of the 2D spectrum obtained with $\tau_{exc} = \tau_{rec}$, using phase-cycles appropriate for either ^{14}N SQ or DQ detection, and the spin echo signal amplitude $S_{spin\text{-}echo}$ of a 1D spectrum obtained without any ^{14}N pulses. For instance, with $R12_3^5R12_3^{-5}$ sequences during $\tau_{exc} = \tau_{rec} = 6\tau_{rot} = 199.8$ µs (30.03 kHz MAS), we have found that in L-alanine at 9.4 T the experimental efficiency of the two-way coherence transfer process is $r = 0.17$ and 0.08 for ^{14}N SQ and DQ, respectively. Without $R12_3^5R12_3^{-5}$ sequences, the RDS for a ^{1}H–^{14}N pair is merely on the order of 0.1 kHz at 9.4 T, thus requiring $\tau_{exc} = \tau_{rec} = 5$ ms if there were no homogeneous T_2' decay. Empirically, the optimum intervals were found to be $\tau_{exc} = \tau_{rec} = 1$ ms if no recoupling is used [10]. Recoupling by $R12_3^5R12_3^{-5}$ sequences allows one to reduce τ_{exc} and τ_{rec} by a factor 5, thereby considerably reducing T_2' losses in these fixed intervals.

The projections (rather than cross-sections) onto the ω_1 axis are shown along the right-hand side of each 2D spectrum in Fig. 2. In the SQ spectra (top row), the $^{14}NH_3^+$ group leads to a ^{14}N powder lineshape which spans about 3 kHz without resorting to any homo-

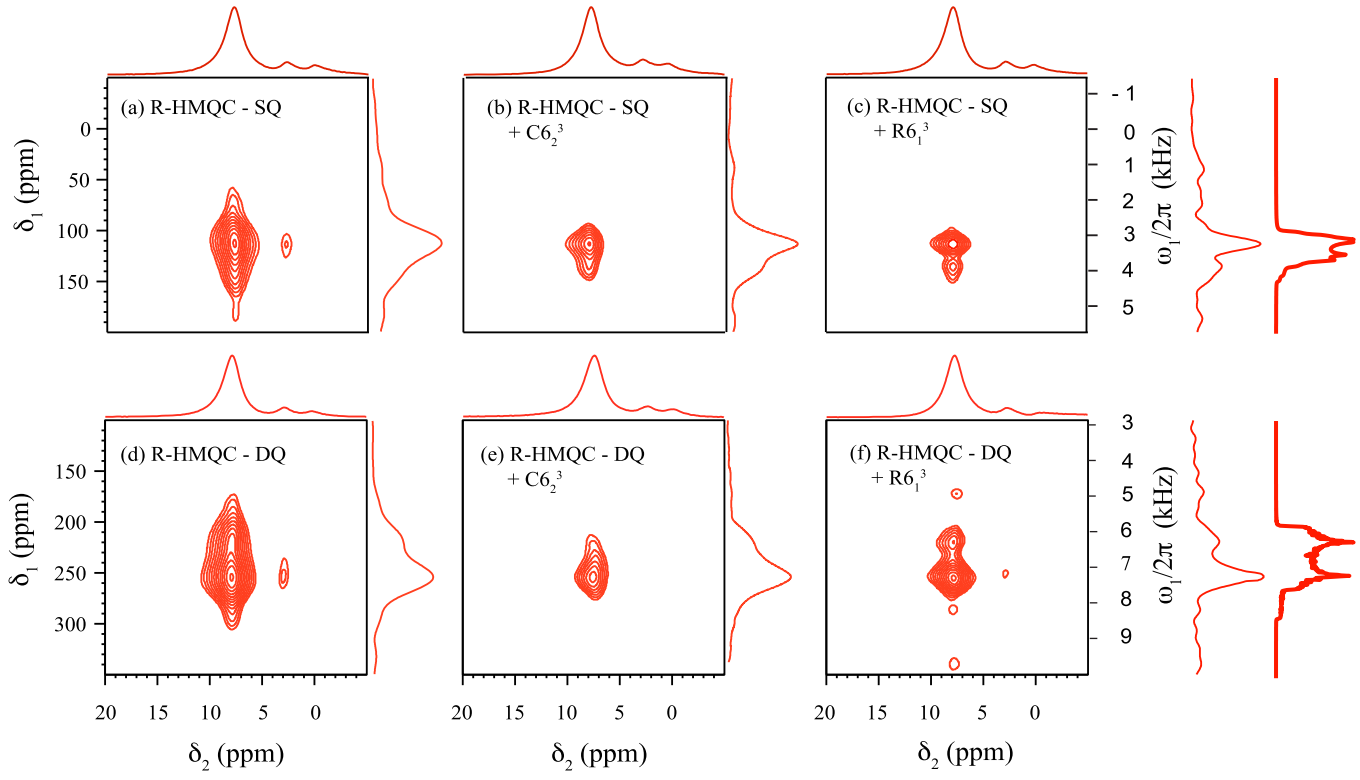

Fig. 2. Experimental R-HMQC spectra showing the ^{14}N SQ (a, b, c) and DQ (d, e, f) responses of the $^{14}NH_3^+$ ammonium group of L-alanine ($^{14}NH_3^+CHCH_3COO^-$) with natural isotopic abundance, i.e., without replacing the remaining protons by deuterium nuclei. A 11 µl sample in a 2.5 mm rotor was spun at 30.03 kHz ($\tau_{rot} = 33.3$ µs) in a static field of 9.4 T (28.9 and 400 MHz for ^{14}N and ^{1}H). The *rf* field amplitudes were $\nu_1(^1H)_{\pi/2} = \nu_1(^1H)_\pi = 120$ kHz and $\nu_1(^1H)_{R12} = 60.06$ kHz in the excitation and the refocusing intervals $\tau_{exc} = \tau_{rec} = 199.8$ µs. Each $R12_3^5$ $R12_3^{-5}$ sequence was comprised of 6 rotors periods. With $\nu_1(^{14}N) = 57$ kHz, the optimum ^{14}N pulse lengths were $\tau_p = 18$ µs for SQ and $\tau_p = 22$ µs for DQ. (a and d) The evolution period t_1 only contains a π^S pulse applied to the protons. (b and e) Before and after the π pulse in the middle of the evolution period $t_1 = n\Delta t_1$, two $R6_1^3$ sequences were inserted. (c and f) Likewise, two $C6_2^3$ sequences were inserted in the evolution period t_1. The simulations of the SQ spectrum (far right) were calculated for $C_Q = 1.13$ MHz and $\eta_Q = 0.28$, assuming uniform excitation of 4180 crystallites, generated with the Zaremba–Conroy–Wolfsberg (ZCW) algorithm [52–54]. The vertical ω_1 axis is calibrated to 0 ppm for NH_4Cl (left side), which coincides with the ^{14}N carrier at 0 kHz (right side). Each of the 2D spectra resulted from averaging 256 transients for each of 64 t_1 increments with $\Delta t_1 = 2/\nu_{rot} = 66.6$ µs for $R6_1^3$ sequences and $\Delta t_1 = 4/\nu_{rot} = 133.2$ µs for $C6_2^3$ sequences. The relaxation interval between consecutive scans was 4 s.

nuclear decoupling in the t_1 evolution period (Fig. 2a), which can be reduced to about 2 kHz by inserting either $C6_2^3$ sequences (Fig. 2b) or $R6_1^3$ sequences (Fig. 2c) in the t_1 evolution interval. Similarly, for DQ spectra (bottom row), the projections onto the ω_1 dimensions shown along the right-hand side of each 2D spectrum, reveal that the $^{14}NH_3^+$ group leads to a signal which spans about 4 kHz (Fig. 2d) that can be reduced to 2.5 kHz by resorting either to $C6_2^3$ sequences (Fig. 2e) or to $R6_1^3$ sequences (Fig. 2f). The spectrum with the greatest similarity to the ideal simulated powder pattern was obtained with the $R6_1^3$ sequence (Fig. 2c and f). However, the spectra obtained with such sequences (Fig. 2c and f) appear to be noisier than those obtained with $C6_2^3$ sequences (Fig. 2b and e). The difference might be due to the nature of the recoupling scheme. Indeed, the $C6_2^3$ sequence gives a scaling factor $k = 0$ for the isotropic chemical shift, whereas the $R6_1^3$ scales the isotropic chemical shift by a theoretical scaling factor $k = 0.45$ with an effective field along the x-axis [22,30,47]. This is represented by a symmetry-allowed first-order rotating-frame average Hamiltonian acting on the protons S during the evolution time t_1

$$\bar{H}^{(1)} = 0.45(\Omega^S S_x + 2\pi J S_x I_z), \tag{2}$$

where Ω^s represents the offset of the proton S with respect to the rf carrier, while J is the scalar coupling constant.

In all these experiments, the C and R sequences are applied to the protons S when the density operator contains terms as S_xI_x, S_yI_x, $S_xI_x^2$ and $S_yI_x^2$. The success of these schemes is not limited to initial states with transverse proton magnetization such as in HMQC-like experiments, but can be extended to initial states with longitudinal proton magnetization such as S_zI_x and $S_zI_x^2$ as occur in HSQC-like experiments [50]. Indeed, the HSQC method offers the possibility

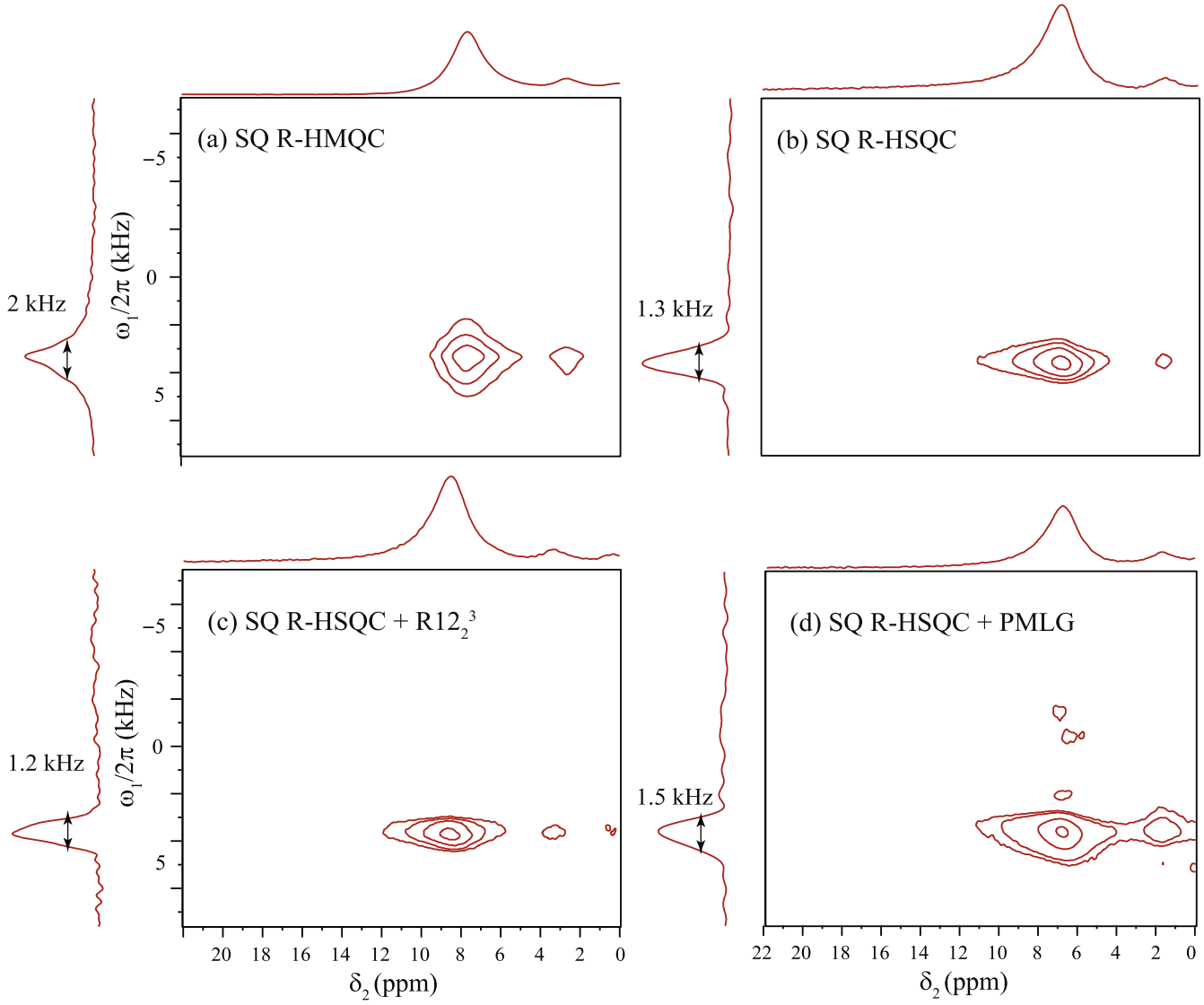

Fig. 3. Experimental spectra showing the ^{14}N SQ responses of the $^{14}NH_3^+$ ammonium group of L-alanine ($^{14}NH_3^+CHCH_3COO^-$). The 2.5 mm rotor was spun at 31.25 kHz (τ_{rot} = 32 μs) in a static field of 9.4 T (28.9 and 400 MHz for ^{14}N and ^1H). The rf field amplitudes were $\nu_1(^1H)_{\pi/2} = \nu_1(^1H)_{\pi} = 120$ kHz and $\nu_1(^1H)_{R12} = 62.5$ kHz in the excitation and the refocusing intervals $\tau_{exc} = \tau_{rec} = 192$ μs. Each $R12_3^5\,R12_3^{-5}$ sequence was comprised of 6 rotor periods. With $\nu_1(^{14}N) = 57$ kHz, the optimum ^{14}N pulse length was $\tau_p = 10$ μs for SQ. (a) Experimental R-HMQC spectra showing a linewidth of 2 kHz in the indirect dimension. (b) Experimental R-HSQC spectra with a linewidth of 1.3 kHz showing a line-narrowing effect compared to the R-HMQC spectra. The evolution period t_1 only contains a π pulse applied to the protons. (c) R-HSQC spectra with $R12_2^3$ symmetry-based homonuclear decoupling during the evolution period t_1. (d) PMLG3$_{pp}^{xx}$ can be implemented in order to decouple homonuclear interactions during the evolution period t_1. The PMLG scheme comprises 12 pulses of 1 μs each, with an rf amplitude of 150 kHz, and a delay of 2 μs between consecutive groups of 6 pulses. The cycle was applied twice, leading to a total duration of 32 μs, corresponding to one rotor period. Each of the 2D spectra resulted from averaging 128 transients for each of 64 t_1 increments. The vertical ω_1 axis is calibrated to 0 ppm for NH_4Cl (left side), which coincides with the ^{14}N carrier at 0 kHz. The relaxation interval between consecutive scans was 3 s.

of implementing rotor-synchronized pulse sequences with time increment given by $\Delta t_1 = \tau_{rot}$, which is not achievable with the HMQC scheme, since a π pulse has to be applied in the middle of t_1, between two rotor-synchronized pulse sequences. Therefore, the HSQC method is preferable, since the spectral width in the indirect dimension is larger.

In this work, we have investigated a series of decoupling schemes in combination with the R-HSQC experiment. This is shown in Fig. 3. Depending on the homonuclear decoupling pulse sequences, different full widths at half maximum (FWHM) have been measured. A remarkable improvement has been observed by comparing R-HMQC with R-HSQC. The FWHM goes from 2 kHz in R-HMQC (Fig. 3a) to 1.3 kHz in R-HSQC (Fig. 3b). The latter can be further reduced to 1.2 kHz (Fig. 3e) by applying homonuclear decoupling schemes such as the $R12_2^3$ during each t_1 increment of the R-HSQC scheme. The $PMLG3^{xx}_{pp}$ scheme, repeated twice per rotor period, did not lead to any remarkable improvement of the resolution (Fig. 3d). We observed a strong dependence of the efficiency of the PMLG scheme upon the proton *rf* carrier frequency, so that a fairly good resolution could be obtained by this method by adjusting the *rf* carrier frequency.

In Fig. 4 we plot the ω_1 projections of the 2D spectra shown in Fig. 3 with simulations of a two-spin system (I, S) under the effects of quadrupolar and other recoupled interactions.

As in Fig. 3, we have investigated the efficiency of $C6_2^3$ and $R6_1^3$ applied in combination with the R-HSQC scheme. While the former does not perform well, the latter introduces an additional chemical shift term that distorts the ^{14}N spectra. The resulting patterns are plotted in Fig. 5 and can be explained by the recoupled first-order chemical-shift average Hamiltonian for ^{1}H (spin S). Under the effect of the symmetry-based sequence $R6_1^3$, we found that the Hamiltonian can be described by

$$\bar{H}_{CS}^{(1)} = k_1\left(\Omega^S T_{11}^S - \Omega^S T_{1-1}^S\right) + k_2 \Omega^S T_{10}^S, \quad (3)$$

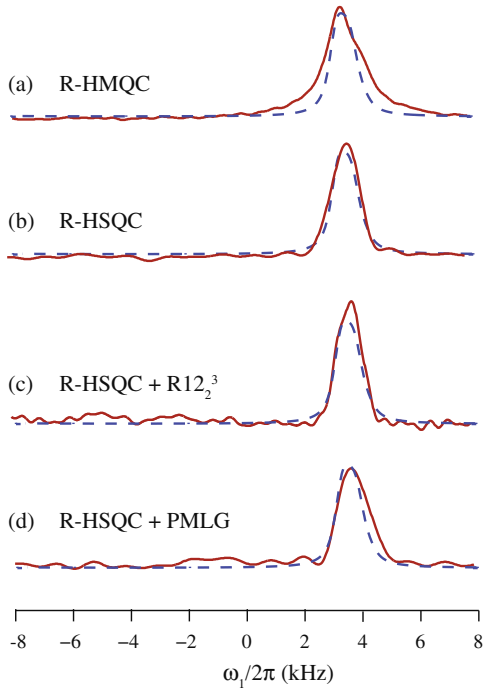

Fig. 4. (a–d) Experimental proton-detected SQ ^{14}N spectra of L-alanine obtained by the projection onto the ω_1 axis of Fig. 3. The dashed lines correspond to simulations (with a line-broadening of 1 kHz) of ^{14}N SQ spectra obtained with $C_Q = 1.13$ MHz and $\eta_Q = 0.28$, and assuming uniform excitation of 4180 crystallites, generated with the ZCW algorithm [52–54].

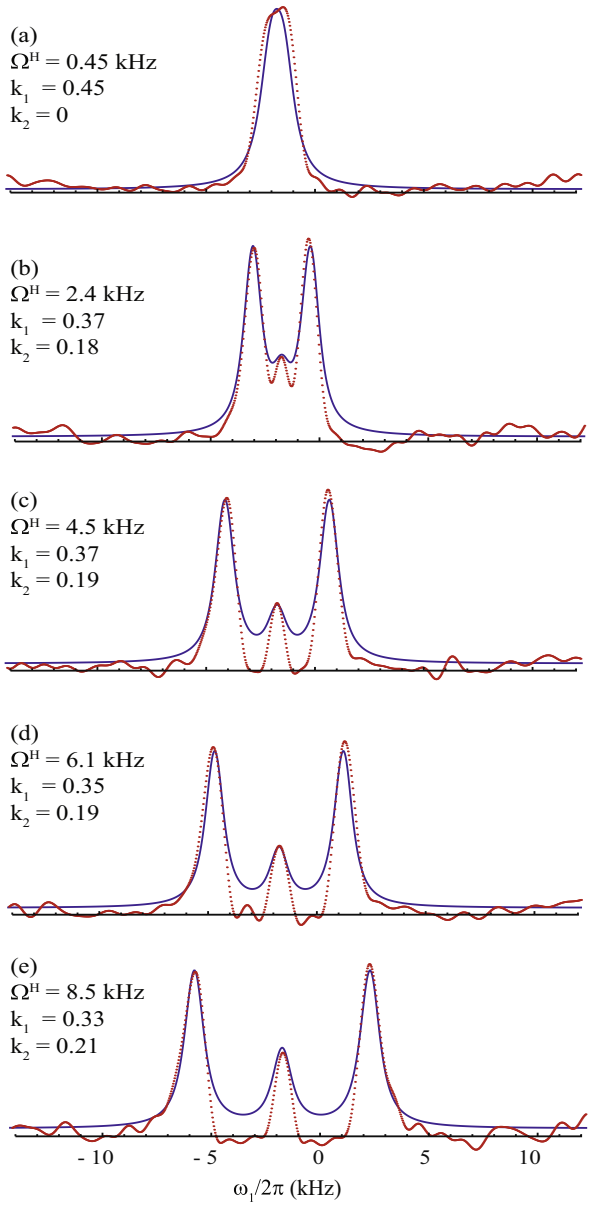

Fig. 5. (a–e) Projections onto the ω_1 axis of experimental 2D proton-detected SQ ^{14}N spectra of L-alanine obtained at 18.8 T (800 MHz for ^{1}H) with 31.25 kHz spinning frequency. The spectra were acquired with different ^{1}H *rf* carriers, i.e., with different ^{1}H offsets Ω^H. The scaling factors k_1 and k_2 refer to Eq. (3). The continuous lines correspond to simulations (with 2.5 kHz line-broadening) of ^{14}N SQ spectra obtained with $C_Q = 1.13$ MHz and $\eta_Q = 0.28$, assuming uniform excitation of 4180 crystallites, generated with the ZCW algorithm [52–54].

where k_1 and k_2 are scaling factors. When the *rf* carrier is set on resonance (Fig. 5a), $k_1 = 0.45$ and $k_2 = 0$, as expected from the theory [21,22]. Far off resonance (Fig. 5b–e), the symmetry-based pulse sequence may be less efficient and consequently the experimental k_1 is smaller than the theoretical value. Further off resonance, we have observed a weak peak half-way between the two more intense peaks (Fig. 5b–e). This "triplet"-like feature can be attributed to small errors of the π pulses used during the $R6_1^3$ pulse sequence that lead to a scaled Zeeman term with $k_2 \neq 0$. In the HMQC scheme, the π pulse in the middle of the t_1 evolution period refocuses the effect of the above Hamiltonian acting on the protons S thus preventing the formation of the "triplet" (Fig. 2c and f).

The R-HSQC sequence was applied to the tripeptide AAG. Good resolution was achieved without applying any decoupling scheme

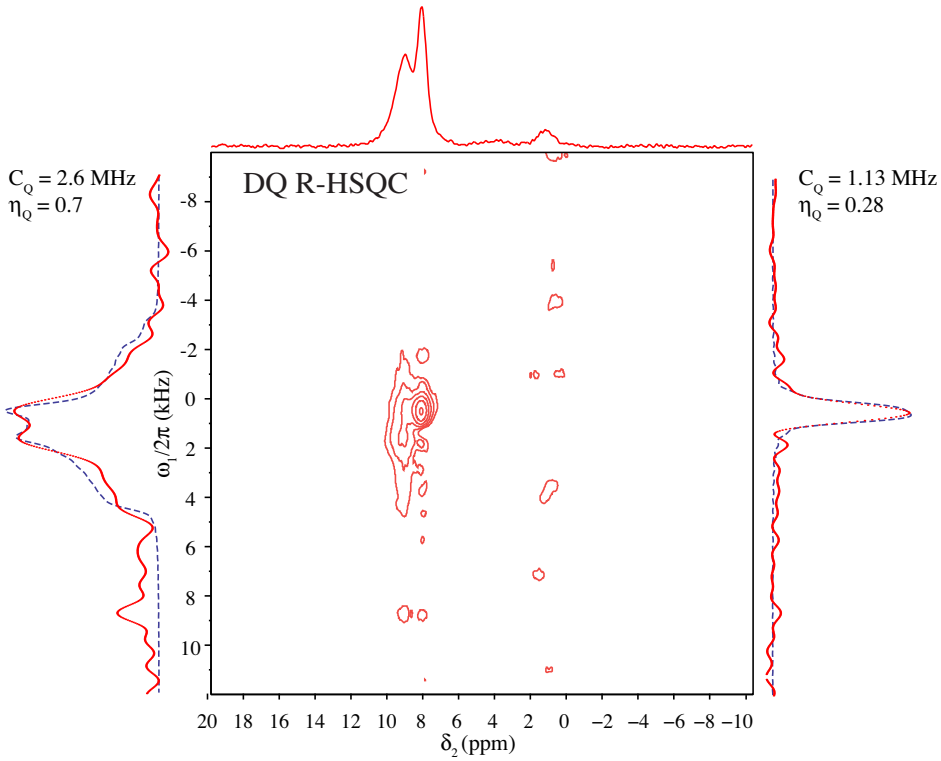

Fig. 6. Experimental and simulated (red continuous and dashed blue lines) R-HSQC spectra showing the ^{14}N DQ responses of AAG ($NH_3^+C^\alpha HCH_3CONHC^\alpha HCH_3CONHC^\alpha H_2COO^-$). The 2.5 mm rotor was spun at 31.25 kHz (τ_{rot} = 32 μs) in a static field of 18.8 T (57.8 and 800 MHz for ^{14}N and ^{1}H). The $R12_3^5$ pulse sequence was applied during 3 rotors periods leading to excitation and refocusing intervals $\tau_{exc} = \tau_{rec}$ = 96 μs. The *rf* field amplitudes were $\nu_1(^1H)_{\pi/2} = \nu_1(^1H)_\pi$ = 120 kHz and $\nu_1(^1H)_{R12}$ = 62.5 kHz in the excitation and the refocusing intervals. With $\nu_1(^{14}N)$ = 57 kHz, the optimum ^{14}N pulse length was τ_p = 20 μs for SQ. The 2D spectra resulted from averaging 512 transients for each of 64 t_1 increments. The vertical ω_1 axis is calibrated to 0 ppm for NH_4Cl (left side), which coincides with the ^{14}N carrier at 0 kHz. The spectrum was acquired with an ^{14}N offset Ω^N = 3 kHz. The relaxation interval between consecutive scans was 3 s. The simulations (with a line-broadening of 1 kHz) of ^{14}N SQ spectra obtained with C_Q = 2.6 MHz and η_Q = 0.7 for the amide ^{14}N in the peptide bond between the two alanine residues and C_Q = 1.13 MHz and η_Q = 0.28 for the ^{14}N of the terminal amino group $-NH_3^+$. We assumed uniform excitation of 4180 crystallites, generated with the ZCW algorithm [52–54].

during t_1. The presence of two amide ^{14}N sites in AAG, characterized by strong quadrupolar interactions (on the order of 2–3 MHz), leads to broad lines, making decoupling unnecessary. Since AAG experiences local dynamics on the 100 nanosecond (ns) timescale [51], we decided to detect the DQ ^{14}N spectrum only, which is not affected by motion. This is shown in Fig. 6. The good match between experiments and simulations at 18.8 T allows one to extract the quadrupolar coupling constant and the asymmetry parameter of two distinct ^{14}N sites (out of three) in AAG. The two detected ^{14}N peaks correspond to the ^{14}N of the $-NH_3^+$ group (C_Q = 1.13 MHz and η_Q = 0.28) of the terminal L-alanine and to the –NH group (C_Q = 2.6 MHz and η_Q = 0.7) in the peptide bond between the two L-alanine residues. The third ^{14}N, which belongs to the alanine–glycine linkage, did not appear in the 2D R-HSQC spectra, possibly because it may have a larger quadrupolar coupling, which would require different conditions.

7. Conclusions

It has been shown that the indirect detection of ^{14}N spectra via protons can benefit from decoupling of homonuclear proton–proton dipolar interactions. The resulting line-narrowing allows one to obtain higher ^{14}N SQ and DQ resolution and to extract more reliable quadrupolar parameters in amino acids and peptides. The experiments proposed in this work should further benefit from the advent of very fast spinning probes with very high *rf* amplitudes, which should improve the performance of all decoupling sequences used in this work. In cases where the ^{14}N SQ powder pattern is affected by motions, HSQC may provide more accurate measurements compared to HMQC, since it reduces the broadening due to strong proton–proton dipolar interactions.

Acknowledgments

This work has been supported by the Swiss National Science Foundation (FNRS Grant 200020-124694) and the Swiss Commission for Technology and Innovation (CTI Grant 9991.1 PFIW-IW).

References

[1] W.G. Proctor, F.C. Yu, The dependence of a nuclear magnetic resonance frequency upon chemical compound, Phys. Rev. 77 (1950) 717.
[2] R.E. Stark, R.A. Haberkorn, R.G. Griffin, N-14 NMR determination of NH bond lengths in solids, J. Chem. Phys. 68 (1978) 1996.
[3] R. Tycko, P.L. Stewart, S.J. Opella, Peptide plane orientations determined by fundamental and overtone N-14 NMR, J. Am. Chem. Soc. 108 (1986) 5419.
[4] H.J. Jakobsen, H. Bildsoe, J. Skibsted, T. Giavani, N-14 MAS NMR spectroscopy: the nitrate ion, J. Am. Chem. Soc. 123 (2001) 5098.
[5] L. Müller, J. Am. Chem. Soc. 101 (1979) 4481.
[6] D. Massiot, F. Fayon, B. Alonso, J. Trébosc, J.P. Amoureux, Chemical bonding differences evidenced from *J*-coupling in solid state NMR experiments involving quadrupolar nuclei, J. Magn. Reson. 164 (2003) 160.
[7] D. Iuga, C. Morais, Z. Gan, D.R. Neuville, L. Cormier, D. Massiot, NMR heteronuclear correlation between quadrupolar nuclei in solids, J. Am. Chem. Soc. 127 (2005) 11540.
[8] Z. Gan, Measuring amide nitrogen quadrupolar coupling by high-resolution N-14/C-13 NMR correlation under magic-angle spinning, J. Am. Chem. Soc. 128 (2006) 6040.
[9] S. Cavadini, A. Lupulescu, S. Antonijevic, G. Bodenhausen, Nitrogen-14 NMR spectroscopy using residual dipolar splittings in solids, J. Am. Chem. Soc. 128 (2006) 7706.
[10] S. Cavadini, S. Antonijevic, A. Lupulescu, G. Bodenhausen, Indirect detection of nitrogen-14 in solids via protons by nuclear magnetic resonance spectroscopy, J. Magn. Reson. 182 (2006) 168.

[11] S. Cavadini, S. Antonijevic, A. Lupulescu, G. Bodenhausen, Indirect detection of nitrogen-14 in solid-state NMR spectroscopy, ChemPhysChem 8 (2007) 1363.
[12] Z. Gan, Rotary resonance echo double resonance for measuring heteronuclear dipolar coupling under MAS, J. Magn. Reson. 183 (2006) 235.
[13] Z. Gan, 13C/14N heteronuclear multiple-quantum correlation with rotary resonance and REDOR dipolar recoupling, J. Magn. Reson. 184 (2006) 39.
[14] Z. Gan, J.P. Amoureux, J. Trébosc, Proton-detected N-14 MAS NMR using homonuclear decoupled rotary resonance, Chem. Phys. Lett. 435 (2007) 163.
[15] R.K. Harris, A.C. Olivieri, Quadrupolar effects transferred to spin-1/2 magic-angle spinning spectra of solids, Prog. NMR Spectrosc. 24 (1992) 435.
[16] J. McManus, R. Kemp-Harper, S. Wimperis, Second-order quadrupolar–dipolar broadening in two-dimensional multiple-quantum MAS NMR, Chem. Phys. Lett. 311 (1999) 292.
[17] M.H. Levitt, T.G. Oas, R.G. Griffin, Rotary resonance recoupling in heteronuclear spin pair systems, Isr. J. Chem. 28 (1988) 271.
[18] T.G. Oas, R.G. Griffin, M.H. Levitt, Rotary resonance recoupling of dipolar interactions in solid-state nuclear magnetic-resonance spectroscopy, J. Chem. Phys. 89 (1988) 692.
[19] Z.H. Gan, D.M. Grant, Rotational resonance in a spin-lock field for solid-state NMR, Chem. Phys. Lett. 168 (1990) 304.
[20] Z.H. Gan, D.M. Grant, R.R. Ernst, NMR chemical shift anisotropy measurements by RF driven rotary resonance, Chem. Phys. Lett. 254 (1996) 349.
[21] M. Carravetta, M. Eden, X. Zhao, A. Brinkmann, M.H. Levitt, Symmetry principles for the design of radiofrequency pulse sequences in the nuclear magnetic resonance of rotating solids, Chem. Phys. Lett. 321 (2000) 205.
[22] M.H. Levitt, Encycl. Nucl. Magn. Reson. 9 (2002) 165.
[23] S. Cavadini, A. Abraham, G. Bodenhausen, Proton-detected nitrogen-14 NMR by recoupling of heteronuclear dipolar interactions using symmetry-based sequences, Chem. Phys. Lett. 445 (2007) 1.
[24] J.D. van Beek, R. Dupree, M.H. Levitt, Symmetry-based recoupling of O-17–H-1 spin pairs in magic-angle spinning NMR, J. Magn. Reson. 179 (2006) 38.
[25] A. Brinkmann, A.P.M. Kentgens, Sensitivity enhancement and heteronuclear distance measurements in biological O-17 solid-state NMR, J. Phys. Chem. B 110 (2006) 16089.
[26] A. Brinkmann, A.P.M. Kentgens, Proton-selective O-17–H-1 distance measurements in fast magic-angle-spinning solid-state NMR spectroscopy for the determination of hydrogen bond lengths, J. Am. Chem. Soc. 128 (2006) 14758.
[27] S.P. Brown, Probing proton–proton proximities in the solid state, Prog. NMR Spectrosc. 50 (2007) 199.
[28] B.C. Gerstein, C. Chow, R.G. Pembleton, R.C. Wilson, Utility of pulse nuclear magnetic-resonance in studying protons in coals, J. Phys. Chem. 81 (1977) 565.
[29] S. Hafner, H.W. Spiess, Multiple-pulse line narrowing under fast magic-angle spinning, J. Magn. Reson., Ser. A 121 (1996) 160.
[30] P.K. Madhu, X. Zhao, M.H. Levitt, High-resolution H-1 NMR in the solid state using symmetry-based pulse sequences, Chem. Phys. Lett. 346 (2001) 142.
[31] S. Paul, R.S. Thakur, P.K. Madhu, H-1 homonuclear dipolar decoupling at high magic-angle spinning frequencies with rotor-synchronised symmetry, Chem. Phys. Lett. 456 (2008) 253.
[32] M. Lee, W.I. Goldburg, Nuclear-magnetic-resonance line narrowing by a rotating *rf* field, Phys. Rev. 140 (1965) A1261.
[33] M. Mehring, J.S. Waugh, Magic-angle NMR experiments in solids, Phys. Rev. B 5 (1972) 3459.
[34] M.H. Levitt, A.C. Kolbert, A. Bielecki, D.J. Ruben, High-resolution 1H NMR in solids with frequency-switched multiple-pulse sequences, Solid State Nucl. Magn. Reson. 2 (1993) 151.
[35] E. Vinogradov, P.K. Madhu, S. Vega, High-resolution proton solid-state NMR spectroscopy by phase-modulated Lee–Goldburg experiment, Chem. Phys. Lett. 314 (1999) 443.
[36] E. Vinogradov, P.K. Madhu, S. Vega, Phase modulated Lee–Goldburg magic angle spinning proton nuclear magnetic resonance experiments in the solid state: a bimodal Floquet theoretical treatment, J. Chem. Phys. 115 (2001) 8983.
[37] M. Leskes, P.K. Madhu, S. Vega, Proton line narrowing in solid-state nuclear magnetic resonance: new insights from windowed phase-modulated Lee–Goldburg sequence, J. Chem. Phys. 125 (2006).
[38] M. Leskes, P.K. Madhu, S. Vega, A broad-banded *z*-rotation windowed phase-modulated Lee–Goldburg pulse sequence for H-1 spectroscopy in solid-state NMR, Chem. Phys. Lett. 447 (2007) 370.
[39] M. Leskes, P.K. Madhu, S. Vega, Supercycled homonuclear dipolar decoupling in solid-state NMR: toward cleaner H-1 spectrum and higher spinning rates, J. Chem. Phys. 128 (2008).
[40] D. Sakellariou, A. Lesage, P. Hodgkinson, L. Emsley, Homonuclear dipolar decoupling in solid-state NMR using continuous phase modulation, Chem. Phys. Lett. 319 (2000) 253.
[41] A. Lesage, D. Sakellariou, S. Hediger, B. Elena, P. Charmont, S. Steuernagel, L. Emsley, Experimental aspects of proton NMR spectroscopy in solids using phase-modulated homonuclear dipolar decoupling, J. Magn. Reson. 163 (2003) 105.
[42] E. Salager, R.S. Stein, S. Steuernagel, A. Lesage, B. Elena, L. Emsley, Enhanced sensitivity in high-resolution H-1 solid-state NMR spectroscopy with DUMBO dipolar decoupling under ultra-fast MAS, Chem. Phys. Lett. 469 (2009) 336.
[43] J.P. Amoureux, B. Hu, J. Trébosc, Enhanced resolution in proton solid-state NMR with very-fast MAS experiments, J. Magn. Reson. 193 (2008) 305.
[44] J.P. Amoureux, B.W. Hu, J. Trébosc, Q. Wang, O. Lafon, F. Deng, Homonuclear dipolar decoupling schemes for fast MAS, Solid State Nucl. Magn. Reson. 35 (2009) 19.
[45] S. Antonijevic, G. Bodenhausen, High-resolution NMR spectroscopy in solids by truly magic-angle spinning, Angew. Chem. Int. Edit. 44 (2005) 2935.
[46] A. Brinkmann, M. Eden, Second order average Hamiltonian theory of symmetry-based pulse schemes in the nuclear magnetic resonance of rotating solids: application to triple-quantum dipolar recoupling, J. Chem. Phys. 120 (2004) 11726.
[47] A. Brinkmann, M.H. Levitt, Symmetry principles in the nuclear magnetic resonance of spinning solids: heteronuclear recoupling by generalized Hartmann–Hahn sequences, J. Chem. Phys. 115 (2001) 357.
[48] M. Leskes, S. Steuernagel, D. Schneider, P.K. Madhu, S. Vega, Homonuclear dipolar decoupling at magic-angle spinning frequencies up to 65 kHz in solid-state nuclear magnetic resonance, Chem. Phys. Lett. 466 (2008) 95.
[49] A. Brinkmann, J.S. auf der Günne, M.H. Levitt, Homonuclear zero-quantum recoupling in fast magic-angle spinning nuclear magnetic resonance, J. Magn. Reson. 156 (2002) 79.
[50] S. Cavadini, A. Abraham, G. Bodenhausen, Coherence transfer between spy nuclei and nitrogen-14 in solids, J. Magn. Reson. 190 (2008) 160.
[51] S. Cavadini, A. Abraham, S. Ulzega, G. Bodenhausen, Evidence for dynamics on a 100 ns time scale from single- and double-quantum nitrogen-14 NMR in solid peptides, J. Am. Chem. Soc. 130 (2008) 10850.
[52] V.B. Cheng, H.H. Suzukawa, M. Wolfsberg, Investigations of a nonrandom numerical-method for multidimensional integration, J. Chem. Phys. 59 (1973) 3992.
[53] H. Conroy, Molecular Schrödinger equation. VIII. A new method for the evaluation of multidimensional integrals, J. Chem. Phys. 47 (1967) 5307.
[54] S.K. Zaremba, Good lattice points, discrepancy, and numerical integration, Ann. Mat. Pure Appl. 4–54 (1966) 325.